

## ● Original Contribution

# LARGE-VOLUME HYPERTHERMIA FOR SAFE AND COST-EFFECTIVE TARGETED DRUG DELIVERY USING A CLINICAL ULTRASOUND-GUIDED FOCUSED ULTRASOUND DEVICE

PAUL CHRISTOPHER LYON,<sup>\*,†,‡</sup> CHRISTOPHOROS MANNARIS,<sup>\*</sup> MICHAEL GRAY,<sup>\*</sup> ROBERT CARLISLE,<sup>\*</sup>  
 FERGUS V. GLEESON,<sup>‡</sup> DAVID CRANSTON,<sup>†</sup> FENG WU,<sup>†</sup> and CONSTANTIN C. COUSSIOS<sup>\*</sup>

<sup>\*</sup> Institute of Biomedical Engineering, University of Oxford, Oxford, UK; <sup>†</sup> Nuffield Department of Surgical Sciences, Oxford, UK; and <sup>‡</sup> Department of Radiology, Oxford University Hospitals NHS Foundation Trust, Oxford, UK

(Received 3 September 2020; revised 3 December 2020; in final form 10 December 2020)

**Abstract**—Lyso-thermosensitive liposomes (LTSLs) are specifically designed to release chemotherapy agents under conditions of mild hyperthermia. Preclinical studies have indicated that magnetic resonance (MR)-guided focused ultrasound (FUS) systems can generate well-controlled volumetric hyperthermia using real-time thermometry. However, high-throughput clinical translation of these approaches for drug delivery is challenging, not least because of the significant cost overhead of MR guidance and the much larger volumes that need to be heated clinically. Using an ultrasound-guided extracorporeal clinical FUS device (Chongqing HAIFU, JC200) with thermistors in a non-perfused *ex vivo* bovine liver tissue model with ribs, we present an optimised strategy for rapidly inducing (5–15 min) and sustaining (>30 min) mild hyperthermia ( $\Delta T < +4^{\circ}\text{C}$ ) in large tissue volumes ( $\leq 92\text{ cm}^3$ ). We describe successful clinical translation in a first-in-human clinical trial of targeted drug delivery of LTSLs (TARDOX: a phase I study to investigate drug release from thermosensitive liposomes in liver tumours), in which targeted tumour hyperthermia resulted in localised chemo-ablation. The heating strategy is potentially applicable to other indications and ultrasound-guided FUS devices. (E-mail: [lyon.hifu@gmail.com](mailto:lyon.hifu@gmail.com)) © 2020 The Author(s). Published by Elsevier Inc. on behalf of World Federation for Ultrasound in Medicine & Biology. This is an open access article under the CC BY-NC-ND license (<http://creativecommons.org/licenses/by-nc-nd/4.0/>).

**Key Words:** Therapeutic ultrasound, Focused ultrasound, High-intensity focused ultrasound, ThermoDox, Lyso-thermosensitive liposomal doxorubicin, Hyperthermia, Drug delivery, Thermometry, Thermal dose, Ultrasound.

## INTRODUCTION

Passive delivery of systemic chemotherapy throughout inoperable solid cancers, including metastases, is hindered by the inability of relatively low circulating drug concentrations to penetrate into the tumour matrix because of high interstitial pressures and poorly perfused regions (Jain 1998, 2012; Bennewith and Dedhar 2011). Lyso-thermosensitive liposomes (LTSLs) are drug delivery systems specifically designed to overcome these limitations by targeted tumour therapy in combination with mild localised hyperthermia (Kong and Dewhirst 1999; Needham et al. 2000).

A decade of research using magnetic resonance (MR)-guided focused ultrasound systems with real-time

thermometry in animal models has revealed that well-controlled volumetric hyperthermia is possible using the real-time feedback and arbitrary motion capabilities of these research systems (Staruch et al. 2011, 2012, 2015). However, clinical translation of these approaches for drug delivery is challenging because of the significant cost overhead of MR guidance, the much larger volumes that need to be heated clinically, the presence of acoustically blocking ribs and the fact that the majority of MR-guided and ultrasound-guided clinical high-intensity focused ultrasound (HIFU) systems today have a much more limited range of motion and exposure settings than research systems.

The key challenge is to sustain the required temperature rise ( $39.5^{\circ}\text{C}$ – $43^{\circ}\text{C}$  for lyso-thermosensitive liposomal doxorubicin [LTLD]) over the entire tumour volume for a duration compatible with the therapeutic circulating time of the drug—some 30–60 min when

Address correspondence to: Paul C. Lyon, Department of Radiology, Churchill Hospital, Old Road, Headington, Oxford OX3 7 LE, UK. E-mail: [lyon.hifu@gmail.com](mailto:lyon.hifu@gmail.com)

considering a long-circulating thermosensitive liposome such as LTLD (ThermoDox, Celsion Corp., Lawrenceville, NJ, USA), the first thermosensitive liposome to be approved for investigational clinical use (Poon and Borys 2009, 2011; Wood *et al.* 2012). Rapid induction of large-volume hyperthermia may not only facilitate pharmacokinetics of the circulating drug but will also reduce procedural time, which is particularly important for practicality of treatment administration, especially so if delivery is performed under sedation or general anaesthesia.

Whilst lacking non-invasive thermometry capabilities, ultrasound-guided focused ultrasound (FUS) systems may offer increased affordability and practicality over magnetic resonance imaging (MRI)-guided devices for delivery of targeted chemotherapy to large numbers of patients. Unlike MR-guided devices, clinically available ultrasound-guided systems typically consist of single-element ultrasound transducers that need to be translated mechanically, rather than transducer arrays with beam-steering capability (Smith *et al.* 1991). These ultrasound-guided systems were designed primarily for ablative therapy (Hill and ter Haar 1995; Kennedy *et al.* 2003; Illing *et al.* 2005), rather than for induction of clinically relevant volumes of hyperthermia. The parameters that can therefore be controlled by the operator are limited to those controlling acoustic output (power, duty cycle [DC]) and FUS source trajectory (speed, scan geometry and sequence). The latter will influence the effective DC, that is, the resultant DC during execution of a HIFU treatment plan over a tumour volume, which will always be lower than the output DC (the DC output from the HIFU device when HIFU exposure is treating a single unit) because of off time whilst the transducer translates between treatment units (either dots or lines).

In this article, we describe the optimization of FUS settings that were possible within the constraints of an approved clinical HIFU device (JC200, Haifu Medical Technology Co., Chongqing, China) to induce rapid (10–15 min) and sustainable (>30 min) large-volume hyperthermia (on the order of 40–100 cm<sup>3</sup>) whilst minimizing the acoustic energy delivery to reduce risks of off-target effects, using an *ex vivo* model both in the absence and in the presence of ribs. The tolerability and feasibility of targeted drug delivery using FUS for hyperthermia-induced release from LTSLs was recently studied in a first-in-human trial (TARDOX study) using the same JC200 ultrasound-guided system, which lacks real-time thermometry capability (Lyon *et al.* 2018; Gray *et al.* 2019). We provide clinical real-time thermometry data from this trial to illustrate how the heating strategies translate clinically.

## METHODS

### HIFU System

*Ex vivo* liver hyperthermia experiments were carried out using an ultrasound-guided clinical CE-marked FUS system (JC200) at the lowest possible acoustic power setting (32 W, as reported by the manufacturer for acoustic power measurement in water) and varying DCs whilst employing a fixed 100-ms pulse interval. The FUS source was a fixed-focus, 20-cm-diameter annular transducer operating at 0.96 MHz. An integral coaxial B-mode probe was used for ultrasound guidance. The clinical HIFU device was calibrated using a needle hydrophone (HNA0400, ONDA Corp., Sunnyvale, CA, USA), and free field pressure at the focus was estimated to be 15.9 MPa peak-to-peak at this power setting

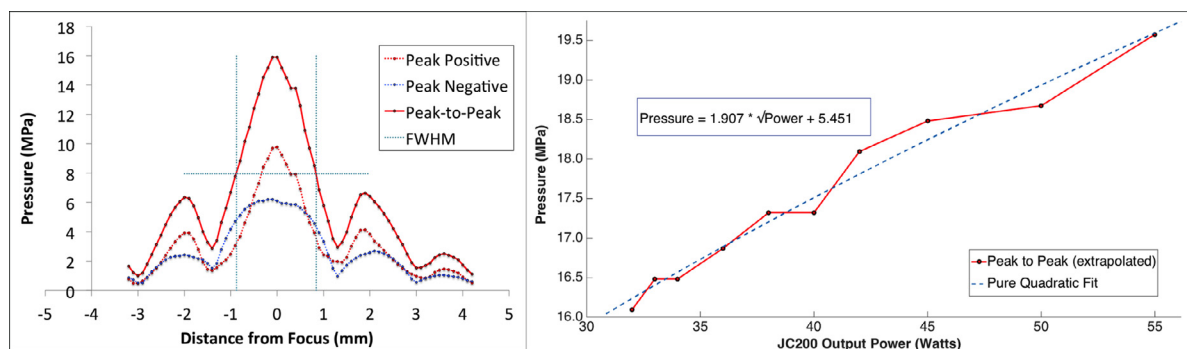


Fig. 1. Left: Pressure amplitude calibration (beam pattern) generated in the axial field by the JC200 at 32 W, 1% duty cycle (DC) and 5-ms pulse repetition frequency (PRF), by manual movements on a calibrated ONDA hydrophone using a 3-D gantry with 0.1-mm resolution in the x-axis only. The full width at half maximum (FWHM) is 1.72 mm, indicated by light blue dotted lines. The maximum pressures at the focus and first side lobe are 15.90 and 6.35 MPa peak-to-peak, respectively. Pressures at the focus may represent an underestimate because of the presence of non-linearity (Lyon 2016). Right: Approximated JC200 calibration based on extrapolation of a calibration performed at the first side lobe, using a 1% DC and 5-ms PRF. Extrapolated peak-to-peak focal pressures, predicting those at the true focus, based on the side lobe calibration. Pure quadratic fit and its equation for the free-field focal peak-to-peak pressures shown. Fit parameters:  $R^2 = 0.9748$ , root mean square error (RMSE) = 0.1902, sum of squares due to error (SSE) = 0.2893.

Table 1. Power converted and derated energy inputs for preclinical experiments (sets 1 and 2) and clinical treatment (set 3)

Expt Set ID	JC200 energy output, $E_{\text{scan}}$ (kJ) adjusted for output DC	Corrected for power conversion efficiency, $E_{\text{scan}}$ (kJ)	Derated for liver tissue, $E_{\text{US}}$ (kJ)	Derated for liver tissue and ribs, where applicable, $E_{\text{US}}$ , ribs (kJ)
1(a)	27.6	22.4	15.1	N/A
1(b)	13.8	11.2	7.6	N/A
1(c)	8.4	6.8	4.6	N/A
1(d)	8.2	6.6	4.5	N/A
2(a)*	8.4	6.8	4.6	2.7
2(b)*	11.8	9.6	6.5	3.9
2(c)	12.5	10.1	6.9	N/A
2(d)*	14.3	11.6	7.9	4.7
3(a)* I.01	21.1	17.1	—	8.4
3(b)* I.04	156.3	126.6	—	50.0

Correction for power conversion efficiency is by manufacturer's quoted factor of 0.81 ( $\Delta_{\text{eff}}$ ). Preclinically, derating because of liver tissue is by a factor of 0.68 ( $E_{\text{US}}$ ), and where ribs are present, a further derating factor of 0.59 is applied ( $E_{\text{US}}$ , ribs), regardless of 39- or 92-cm<sup>3</sup> scan volume. Clinically, based on a non-linear model and available computed tomography data, the patient derating factors, including incident tissue and ribs ( $E_{\text{US}}$ , ribs), were 0.49 and 0.39 for treatments 3(a) and 3(b), respectively, equating to 0.40 and 0.32 after correction for power conversion efficiency ( $\Delta_{\text{eff}}$ ).

\* Ribs present.

( $\pm 12\%$  calibration uncertainty at this frequency) (Fig. 1) (Lyon 2016).

First-order estimates of FUS field derating were made to account for tissue attenuation and rib effects that reduce the energy incident upon the heating target. The attenuation derating factor was found from a depth-averaged calculation at 0.96 MHz using

$$\Delta_{\alpha} = \frac{1}{N} \sum_{i=1}^N \exp(-2\alpha_{0.96} z_i) \quad (1)$$

where  $\alpha_{0.96}$  is the attenuation in liver (taken as 0.066 Np/cm at 0.96 MHz [Hasgall et al. 2018]),  $z_i$  are the depths in each scan and  $N$  is the number of tissue depths in a scan.

Transmission loss caused by the presence of ribs was estimated by examining the proportion of the incident beam that would be blocked at each depth and scan line position (PBT( $x_j, z_i$ )). A bounding estimate was found by assuming any blocked sound would not contribute to the field at the targeted location (McGough et al. 1996). A cumulative rib derating factor for each scan was found from the spatial average

$$\Delta_{\text{ribs}} = \frac{1}{MN} \sum_{i=1}^N \sum_{j=1}^M \text{PBT}(x_j, z_i) \quad (2)$$

where  $x_j$  are the positions along each scan line. Here it is assumed that each rib cross-section and its position relative to adjoining ribs are invariant in the y-direction (perpendicular to the long axis of the ribs, parallel to the scan slices).

A more thorough approach would calculate the derating factors using a non-linear model to capture the harmonic generation and absorption in the liver, along with explicit modelling of ribs and cartilage to capture relevant effects for the experiments in this study (e.g.,

scattering, refraction, absorption). However, prior estimates (Gray et al. 2019) suggest that non-linear contributions to heating are small when operating the JC200 at the low powers used in the present study.

Finally, input energy values provided by the JC200 user interface ( $E_{\text{scan}}$ ) were scaled by the manufacturer's value for power conversion efficiency for the FUS source ( $\Delta_{\text{eff}} = 0.81$ ). *In situ* energies for each scan were then estimated without and with the ribs using the factors (Table 1):

$$E_{\text{US}} = E_{\text{scan}} \cdot \Delta_{\text{eff}} \cdot \Delta_{\text{att}} \quad (3a)$$

$$E_{\text{US, ribs}} = E_{\text{scan}} \cdot \Delta_{\text{eff}} \cdot \Delta_{\text{att}} \cdot \Delta_{\text{ribs}} \quad (3b)$$

Energy values reported in this article are presented as input energy corrected for DC/derated energy (kJ) and therefore represent estimates of acoustic energy and are minimally dependent on the specific device used for the present study (allowing for the given transducer geometry, trajectory and heating strategy used).

### Tissue preparation

Preclinical hyperthermia experiments were carried out using fresh *ex vivo* bovine liver obtained within 4 hours of slaughter from a local abattoir. Peripheral regions, avoiding large portal vessels, were sectioned to appropriate size, degassed in phosphate-buffered saline for 1 h and, whilst under saline, loaded in layers into a custom Delrin holder of internal dimensions 10 × 10 × 10 cm, with a 50- $\mu\text{m}$ -thick acoustically transparent Mylar window beneath (Fig. 2). A fresh section of porcine rib cage (mean rib width  $\sim 19$  mm, mean rib space  $\sim 15$  mm) was degassed and secured over the acoustic window to mimic acoustic shielding effects of the human rib cage, as utilised in other pre-clinical HIFU studies (Liu et al. 2010;

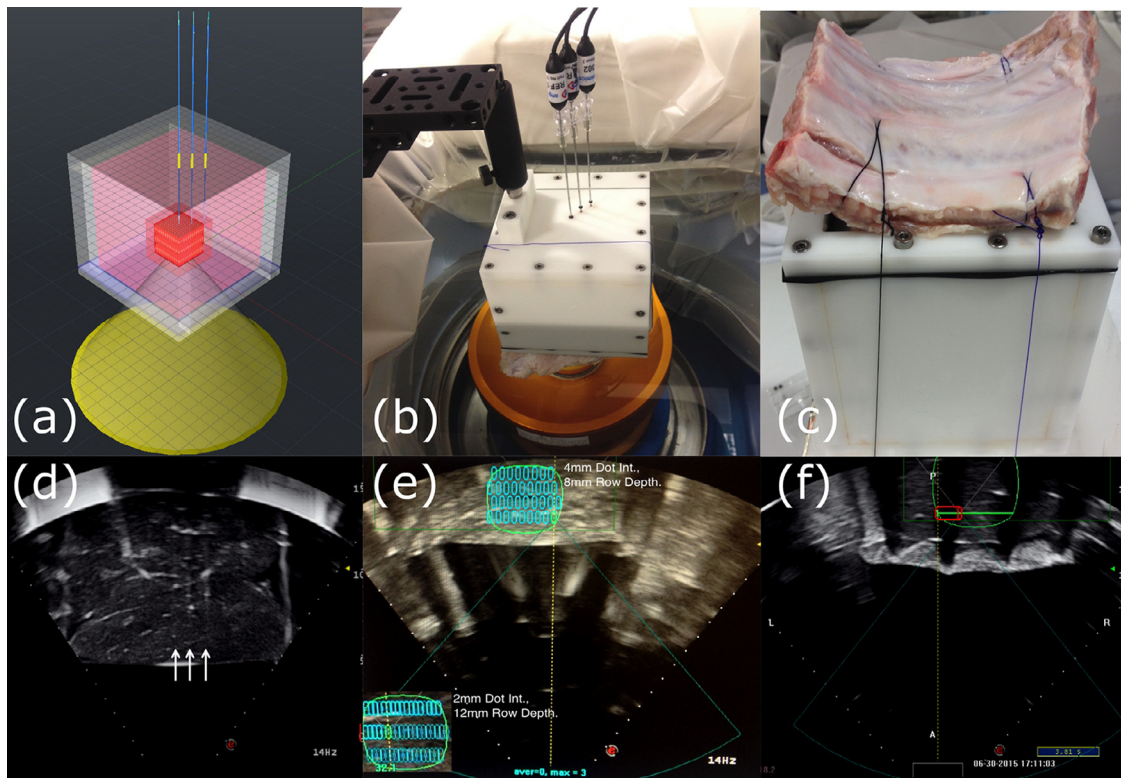


Fig. 2. Experimental setup for co-axial thermistor configuration. (a) Three-dimensional schematic of custom holder (white), containing liver (pink) positioned over the JC200 transducer (yellow). The positions of the central target volumes are indicated in the liver (opaque red  $3 \times 3 \times 3$ -cm cube, semitransparent  $4 \times 4 \times 4$ -cm cube), and the inner, smaller target volume is covered with dot mode focused ultrasound (FUS) exposures for illustration. Both of these cubic heating volumes are spanned with co-axially loaded thermistors (blue) with respect to the direction of FUS and the peripheral thermistor is on the cube edge for  $3 \times 3 \times 3$  cm and just within the cube for  $4 \times 4 \times 4$  cm. Schematic produced using an acoustic cone with a base diameter of 20 cm and a height of 15 cm, closely matching that of the FUS output from the JC200 transducer used for *ex vivo* experiments. (b) Experimental setup on JC200 device, indicating positioning rig and partial immersion into water bath (full immersion was not practical). Note that all thermistors were inserted through 18G co-axial needles to the same axial depth. “O”-Ring rubber washers were applied to co-axial needles to limit thermistor movement. (c) Underside of holder revealing the attachment of degassed ribs to overlay the acoustic window using surgical sutures, used in a subset of the experiments only. (d) B-Mode images captured by the JC200 device during co-axial configuration experiment (without rib application). Three co-axial needles are observed entering the liver co-axially, with the acquisition probe at  $45^\circ$  rotation to capture all three devices in a single B-mode. The thermistor tips themselves cannot be clearly distinguished; only the co-axial needle shafts that contain the thermistors are seen. (e) Example of a single slice of a  $39\text{-cm}^3$  treatment plan covered by dot mode with 4-mm dot separation and 8-mm row separation. Bottom left inset: 2-mm dot separation and 12-mm row separation for comparison, taken from experiment set 1(b). The transducer has completed the slice and is currently on the last unit of the slice. (f) Experiment 2(d). Rib shadowing is seen for each of the four ribs in the rib cage section, which are aligned at  $90^\circ$  to the diagnostic probe. Note the linear mode sweep is in progress (red oval), with the transducer translating to the right at 6 mm/s, and the focus is just about to enter the next intercostal space. In this system, the FUS beam does not turn on and off selectively over ribs and their spaces, and energy is delivered indiscriminately according to the treatment plan, which encompasses a  $92\text{-cm}^3$  prescribed volume in this case.

Khokhlova *et al.* 2014; Chao *et al.* 2015) (Fig. 2). Detailed design schematics of the custom holder are available with measurements (Lyon 2016). A 3-D positioning rig was attached to the bed of the therapeutic device, enabling the holder to be suspended and translated in the water bath above the JC200 transducer. Care was taken to remove any interface air bubbles before commencing FUS experiments.

#### Temperature measurement

Clinically approved thermistors (Acculis Accu5i MTA Temperature Probe, 18G, Ref. 900-304, AngioDynamics, Latham, NY, USA) were used to acquire pre-clinical and clinical thermometry. The thermistors were first characterised to determine the most thermally sensitive region of the device's tip (Lyon 2016). In brief, a 1.1-MHz fixed-focus FUS device (H-102, outer active



diameter = 64.0 mm, inner diameter = 22.0 mm,  $F = 62.64$  mm, 1.7- and 13.0-mm lateral and axial half-amplitude full-width beam widths, respectively; Sonic Concepts, Woodinville, WA, USA) was used to expose the device to single ultrasound bursts at 2-mm increments in distance from the tip, when aligned perpendicularly to the direction of the FUS focus. Temperature elevation was recorded at high temporal resolution (100 Hz) using custom LabView software and a data acquisition unit (HP Agilent 34970A) (Lyon 2016).

In the preclinical heating experiments, a fibre-optic hydrophone (FOH) (Precision Acoustics, Dorset, UK) was also used in close proximity to the thermistors to further validate readings, given the known potential for viscous heating artefact with clinically approved thermistors and thermocouples (Hynnen et al. 1983; Morris et al. 2008).

Both the thermistors and FOH were inserted through clinically approved coaxial needles (18G Temno Evolution biopsy system, Ref. CTT1820, CareFusion, Beckton Dickinson, Franklin Lakes, NJ, USA), using external O-ring rubber washers in the *ex vivo* model to minimise needle movement (Figs. 2 and 3). In all cases, insertion was performed with measurements such that the most temperature-sensitive region of the device tip was placed centrally in the treatment volume in the axial dimension with no co-axial shielding. The clinical cases used the same co-axial needle configuration, without the

use of washers, allowing for repeated insertions and biopsies (Lyon et al. 2017).

### Preclinical experimental setup

For ultrasound-mediated temperature elevation experiments, the JC200 water bath, which contains the FUS and diagnostic transducers, was filled with degassed water at room temperature (19.5°C). This temperature was chosen so that the partially submerged liver model could equilibrate to both room and water temperature throughout before commencing FUS heating. Complete submersion was not possible because of the limited depth of the water bath (Figs. 2 and 3).

The B-mode guidance feature of the JC200 was used to align the focus of the FUS transducer to the co-axially loaded reference thermistor, which was positioned using the rig such that the most thermally sensitive region was at the geometric centre of the heating cube. Single 1-s stationary exposures (“single shots”) at the lowest power (32 W) and low DC (5%–10%) were then used to align to the reference thermistor in three axes using thermal response with greater accuracy (the JC200 positioner is accurate to 1 mm in all coordinates). The reference thermistor was used to obtain the bulk tissue temperature, and all other thermistors and the FOH were used to measure off-centre and peripheral temperatures.

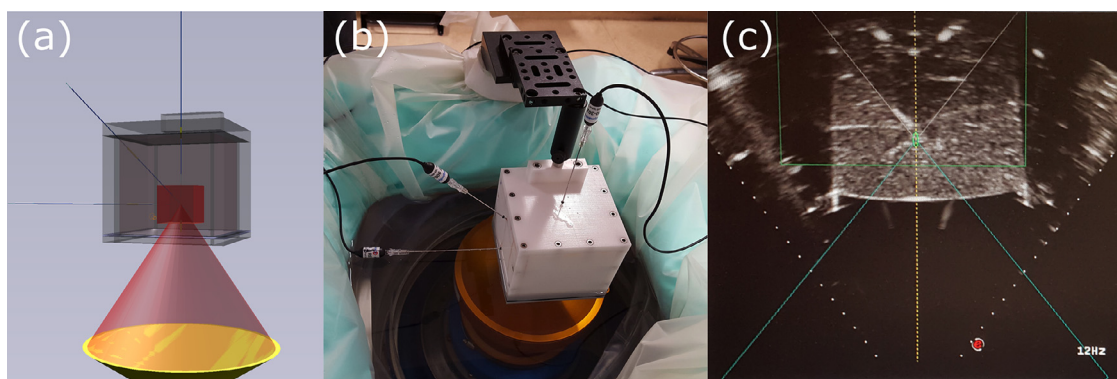


Fig. 3. Experimental setup for multi-angled thermistor configuration (0°, 45° and 90° to focused ultrasound [FUS] device axis). (a) Three-dimensional schematic of custom holder (white), containing liver (pink) positioned over the JC200 transducer (yellow). The position of the center target volume is indicated in the liver (red  $4 \times 4 \times 4$ -cm cube) and is spanned by thermistors (blue) orientated at 0°, 45° and 90° relative to the direction of FUS. All three thermistors are aligned in the same slice. (b) Experimental setup on JC200 device without ribs before the water level was brought up. Air trapped when bringing the water level up was removed using a syringe, and smaller air bubbles at the interface were also removed. “O”-Ring rubber washers were applied to co-axial needles to limit thermistor movement. (c) B-Mode images captured by the JC200 device during multi-angled configuration experiment (without rib application). Co-axial needle and thermistor are shown entering the liver from the top left at 45°, with the high-intensity focused ultrasound focus approximately near the tip of the thermistor. The horizontal line entering the liver from the left represents the orthogonally orientated coaxial needle and thermistor. The co-axially loaded thermistor is not shown as the diagnostic B-mode could not penetrate past the 45° thermistor in this slice (note the echo-poor region above it). Also note the thin echogenic near-horizontal line to the right side of the thermistor tip, which represents the interface between two degassed liver sections layered to fill the holder.

Table 2. Summary of *ex vivo* hyperthermia experiments performed on the JC200

Expt Set ID	Thermistor configuration	Planned/ prescribed volume* (cm <sup>3</sup> )	Mode	Dot interval (on:off:int.)/linear speed	No. of treatment cycles completed (output duty cycle for each <sup>†</sup> )	Ribs present (Y/N)?	Figure
1(a)	Co-axial	27/39	Dot	1 s:1 s:2 mm	1 (100%)	N	4a
1(b)	Co-axial	27/39	Dot	1 s:1 s:4 mm	1 (100%)	N	4b
1(c)	Co-axial	27/39	Linear	6 mm/s	2 (25%, 25%)	N	4c
1(d)	Co-axial + FOH	27/39	Linear	6 mm/s	4 (25%, 10%, 8.6%)	N	4d
2(a) <sup>‡</sup>	Co-axial	27/39	Linear	6 mm/s	2 (25%, 10%, 8.6%)	Y	5a
2(b) <sup>‡</sup>	Co-axial	27/39	Linear	6 mm/s	3 (50%, 10.8%)	Y	5b
2(c)	Multi-angled	64/92	Linear	6 mm/s	0.38 (50%), 0.62 (20%)	N	5c
2(d) <sup>‡</sup>	Co-axial	64 / 92	Linear	6 mm/s	0.5 (50%), 0.5 (20%)	Y	5d
3(a) <sup>‡</sup>	Oblique	—/10.5	Dot	6 mm/s	1.2 (100%)	Y	6a
3(b) <sup>‡</sup>	Oblique	—/73.4	Linear	6 mm/s	2.4 (50%, 38%, 50%)	Y	6b

DC = duty cycle; Expt = experiment; FOH = fibre-optic hydrophone.

The device's minimum output acoustic power of 32 W was used with a pulse interval of 100 ms/10 Hz, a slice thickness of 2 mm and a row distance (minimum depth interval) of 12 mm in all cases.

\* The intended volume for coverage by FUS, on which the modeling and thermistor positioning was based. The resultant prescribed volume reported by the JC200 refers to the volume, which is bounded by user-defined coordinates, is used to generate FUS treatment plans and is independent of the treatment plan parameters. In practice, the prescribed volume is larger than the user-defined treatment volume with straight edges because the JC200 software interpolates more clinically applicable curved edges ("squirrel"), resulting in expansion of the volume. In these experiments, the 27-cm<sup>3</sup> planned volume resulted in a prescribed volume of 39 cm<sup>3</sup>, whilst the 64-cm<sup>3</sup> planned volume had a prescribed volume of 92 cm<sup>3</sup>.

† The output duty cycle (DC) refers to the DC of the HIFU device when HIFU is "on." The output DC will naturally be higher than the effective duty cycle; for example, dot mode was performed as 1 s on, 1 s off, and with approximately 1 s of movement time, continuous wave (100% DC) is reduced to around 25%. In linear mode, there is much less off time and the effective duty cycle is around 65% of the prescribed duty cycle, which is apparent from the thermometry plots. The geometry of the prescribed volume will lead to variations in the effective DC.

‡ Ribs present.

Treatment plans (3-D volume) were defined using the JC200 user interface, to include the most sensitive part of the reference thermistor at its geometric centre. Subsequently, with user-defined parameters, sonication of the planned volumes was automatically controlled using a series of transducer translation paths forming multiple rows over several slices. A single treatment cycle refers to completion of an automated heating plan painting across the tumour volume just once.

The JC200 can generate plans for both dot mode (single-shot exposures between successive transducer movements) and linear mode (continuous row exposures during transducer movement). In linear mode, there is no dwell time at any point in space during sonication of a row of any slice. To form rows in linear mode, the JC200 moves the transducer from the start position on any given row to the end of that row and back to the start position, whilst exposing to FUS at a (configured maximum) fixed speed (6 mm/s), before stopping FUS to move onto the next row. This is contrary to dot mode, which has a minimum exposure (dwell) time of 1 s between exposures and proceeds sequentially without re-treating any units in the same treatment cycle. Both methods were explored at various treatment parameters to optimise speed and maintenance of induction of hyperthermia.

Target cubic volumes of edge length 3 and 4 cm were contoured within the liver model using the device's user interface. This resulted in the generation of a slightly larger prescribed volume of 39 or 92 cm<sup>3</sup> by the

JC200 (see Table 2 footnote for information on planned vs. prescribed volume). The prescribed volumes were then exposed to FUS using automated plans generated by the JC200 user console. In both cases, clipping of the acoustic field by the edges of the acoustic window of the holder was negligible (Lyon 2016). By use of either dot or linear mode, eight individual hyperthermia experiments were carried out as detailed in Table 2. Each experiment consisted of one or more complete treatment cycles, with modifications to the DC either midcycle or between cycles as indicated. As a result of only low levels of hyperthermia, in some cases, within the same experiment set, a single liver model was re-used for two experiments, after being allowed to equilibrate to room and water bath temperature before proceeding to the next experiment. In addition to monitoring B-mode for the absence of gray-scale changes during FUS exposure (which would be consequent with ablation [Ren *et al.* 2007; Wang *et al.* 2012; Lyon *et al.* 2020]), livers were sectioned after experiments to verify lack of macroscopic ablative changes. The examination was performed by dissecting *ex vivo* liver tissue into quarters initially, followed by further sectioning at axial depths of small intervals (<1 cm).

#### Clinical trial approvals

The Health Research Authority National Research Ethics Service, the Oxford University Hospitals Research and Development Department and the UK's Medicines and Healthcare Products Regulatory Agency

granted ethics and regulatory approvals. Patients were recruited from the early phase trials clinic at the Churchill Hospital. All patients gave written consent for study participation.

#### *Clinical treatment setup*

Clinical hyperthermia exposures were carried out similarly to the preclinical experiment, using the same FUS device but at greater power (50–140 W) and with varying DC (30%–100%) but otherwise the same treatment parameters for both dot and linear modes (including transducer speed, unit spacing, slice thickness and motion path). Clinical exposure derating factors were calculated using a treatment planning model employing 3-D calculations of ultrasound propagation and heating (Gray et al. 2019).

Clinical hyperthermia treatments proceeded with the patients under general anaesthetic, using high-frequency jet ventilation to minimise respiratory movement of the liver (Lyon et al. 2017). In each case the visible tumour contour, which was visualised through an intercostal space, was mapped in a slice-by-slice fashion to produce a conforming 3-D volume. In the first clinical experiment presented, which employed dot mode to heat a small tumour of prescribed volume  $10.5 \text{ cm}^3$ , a thermistor tip was placed centrally within the tumour volume, and a second thermistor tip was placed just outside the tumour volume at the tumour margin. The second clinical treatment presented employed linear mode to heat a larger tumour of volume of  $73.4 \text{ cm}^3$ , with a single thermistor placed centrally within the tumour volume (Lyon et al. 2018). In both clinical cases, the thermistors were orientated obliquely to the axis of the HIFU transducer. In contrast to the preclinical experiments, the water within the water bath, in which the patient was partially immersed, was cycled at a lower temperature of  $12^\circ\text{C}$ – $13^\circ\text{C}$  to minimise risk of superficial skin burns at the higher powers employed.

#### *Heating protocols*

Even at a fixed power setting, several other exposure settings on the clinical HIFU device need to be determined, including transducer movement speed (1–6 cm/s), DC and motion path to span the intended treatment volume. The experiments were set up to identify an ultrasound exposure protocol that deposited the minimum total acoustic energy into the tissue to raise the temperature of a clinically relevant volume by between  $4^\circ$ – $8^\circ$  within a matter of minutes and sustain such hyperthermia for a minimum of 30–60 min.

With use of the instrumentation and methods described above, two sets of preclinical experiments were designed to evaluate strategies for volume heating. The purpose of the first set of experiments was to explore the utility of linear mode over dot mode and not necessarily to control the temperature within the tight limits, especially given the absence of ribs. The purpose of the

second set of experiments was to optimise the chosen mode strategy in the presence of ribs and over larger volumes, for up to an hour of hyperthermia, with varied thermistor trajectory, more closely reflecting how the heating protocol might work in clinical practice.

The  $39\text{-cm}^3$  prescribed target volume spanned a 3-cm depth from the acoustic window (1.5–4.5 cm), whilst the  $92\text{-cm}^3$  target volume spanned a 4-cm depth (1–5 cm) with the geometric centres overlaid. Treatments were carried out slice-by-slice with slice thickness (distance between vertical planes) of 2 mm, resulting in 16 slices of three rows each for  $39 \text{ cm}^3$  and 21 slices of four rows for  $92 \text{ cm}^3$  (Fig. 2). Slice separation of four was used in all experiments as a method to trap heat, meaning that after any given slice, the next three were skipped, before resuming the heating plan, which cycled back to the early slices rather like a modulo function. To form rows in single-shot (dot) mode, a 2-mm dot interval was used in experiment set 1(a), followed by a wider (and quicker) 4-mm dot interval in experiment set 1(b). The selected spacings were chosen to exceed the lateral beam-width (1.7-mm full width half-maximum pressure) to minimize the likelihood of overheating regions between adjacent dots and slices. In linear mode, the transducer was translated at the JC200's maximum speed of 6 mm/s.

Clinical cases proceeded similarly with 11 slices for the smaller tumour and 21 slices for the larger tumour, again using 2-mm slice separation. Tumour depths from the skin were 35–58 and 48–124 mm, respectively (Lyon et al. 2018) (see Supplementary Data, online only). Matched parameters of a 2-mm dot interval were used for experiment set 3(a) in dot mode and 6 mm/s translation for experiment set 3(b) in linear mode.

#### *Data analysis*

Real-time thermometry traces were plotted with summary statistics, including mean temperature increase and cumulative equivalent in minutes at  $43^\circ\text{C}$  (CEM43) (Sapareto and Dewey 1984), both centrally and peripherally, using a custom MATLAB client (Lyon 2016). For preclinical cases, CEM43 required a physiologic offset such that the baseline temperature was reset from room temperature to  $37^\circ\text{C}$ . Time to meet a nominal  $\Delta T$  threshold of  $4^\circ\text{C}$  was determined, which is consequent with release of LTLD ( $41^\circ\text{C}$ ) and lies comfortably within the optimal range for release ( $39.5^\circ\text{C}$ – $43^\circ\text{C}$ ). Traces were examined to assess if the temperature elevation could be sustained across multiple treatment cycles.

## RESULTS

#### *Derating factors*

The soft tissue attenuation derating estimates for the model (0.676 and 0.679) were nearly identical for the

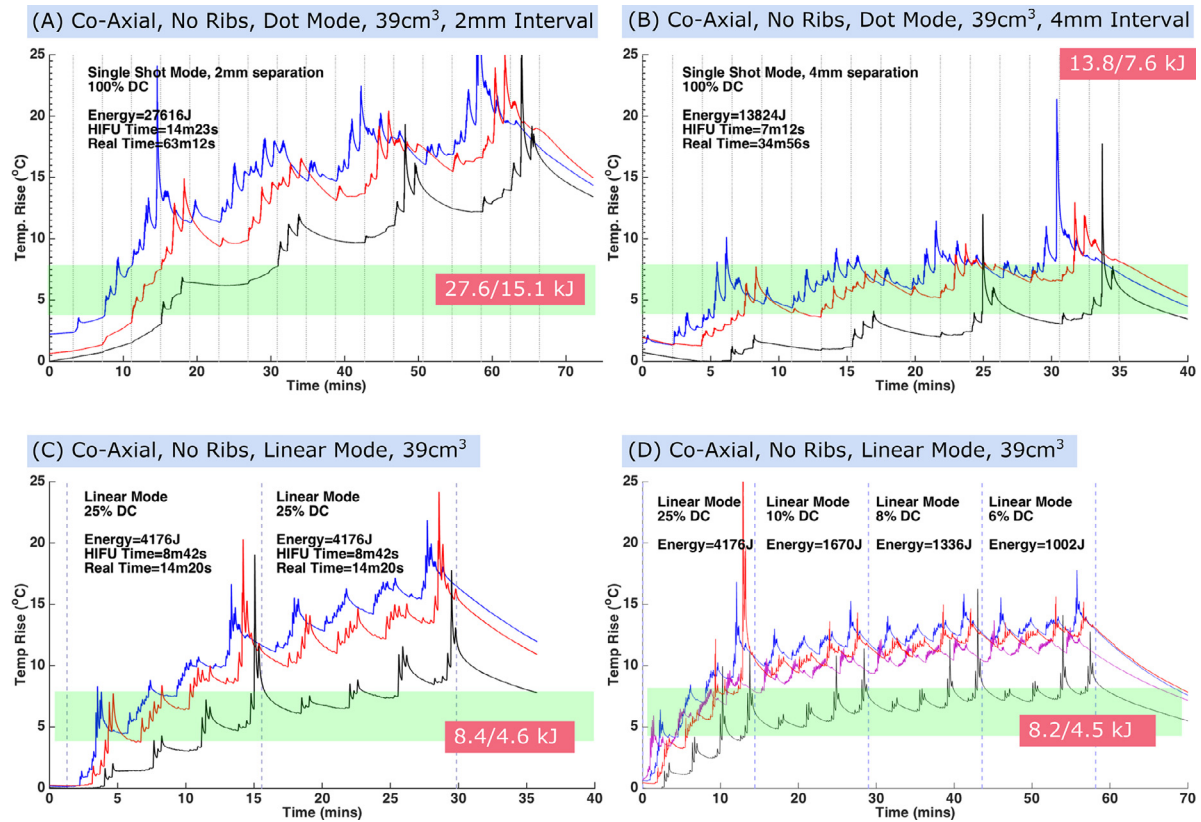


Fig. 4. Thermometry traces obtained from several *ex vivo* liver preparations in the absence of ribs, expressed as a temperature increase ( $\Delta T$ ) from room temperature. All plots were obtained in co-axial thermistor configuration (Fig. 1). Green shaded regions represent the target range of hyperthermia ( $\Delta T = 4^{\circ}\text{C} - 8^{\circ}\text{C}$ ). The blue trace represents the centrally located reference thermistor; the black trace, the peripheral thermistor; the red trace, the thermistor equidistant between them, and the purple trace, the fibre-optic hydrophone. Grey dotted lines in (a) and (b) represent different treatment slices, and horizontal blue dashed lines in (c) and (d) represent start and end of focused ultrasound cycles. Energy inputs are displayed as *a/b* kJ, where *a* = input energy obtained from JC200 treatment reports generated on JC200 device (high-intensity focused ultrasound [HIFU] seconds \* watts) and subsequently corrected for duty cycle (DC), and *b* = energy derated for soft tissues and ribs where present. HIFU time refers to time when the transducer is delivering energy as if continuous wave and disregards DC. (a, b) Comparison of single shot mode (one cycle, 1 s on, 1 s off, ~2-s translation steps of 2 mm with continuous wave during “on” time [i.e., 100% DC decreasing to around 25% effective DC]) using 2-mm (a) or 4-mm (b) dot separation. (c, d) Multiple treatments in linear mode, demonstrating the utility of DC modifications to induce and sustain central and peripheral hyperthermia. In particular, (d) indicates maintenance of a prolonged period of stable hyperthermia (up to 1 h) by repeated cycles and validates thermistor temperature measurements by fibre-optic hydrophone (purple trace).

two preclinical scan volumes (39 and 92 cm<sup>2</sup>, respectively), presumably because the two scans were centred at the same tissue depth and the bounding depths differed only by  $\pm 0.5$  cm. Similarly, the rib derating estimates were 0.592 and 0.595 for the two scan volumes (corrected for depth and frequency), indicating that the spatially averaged effect of scanning across several rib spaces tends to blend out local differences that may exist because of variations of offsets of the intercostal spacing. The estimated derating terms for the clinical cases were 0.49 and 0.39 for experiments 3(a) and 3(b), respectively, as determined from the treatment planning model.

#### Experiment set 1: Effect of sonication mode

Figure 4 illustrates temperature histories for linear-versus-dot mode experiments using the model, along with the target elevation ( $\Delta T$ ) range shown in green and exposure metrics in the upper left. Thermometry summary statistics are summarised in Table 3. The use of dot mode transducer motion with a 2-mm dot interval (trans-axial separation, Fig. 2) and a row separation of 12 mm (resulting in three rows) took more than an hour to span the entire 39-cm<sup>3</sup> prescribed volume target (27 cm<sup>3</sup> planned, see Table 2 footnote) (experiment 1a, Fig. 4a) and required 27.6/15.1 kJ of energy. This time frame limits



Table 3. Summary statistics of the thermometry results of the hyperthermia experiments

Expt Set ID	Time to reach threshold temperature, $\Delta T = 4^\circ\text{C}$ (min)		Mean temperature elevation during exposure ( $\Delta T^\circ\text{C}$ or absolute*)		Physiologic CEM43 (min)	
	Centrally	Peripherally	Centrally	Peripherally	Centrally	Peripherally
1(a)	7.50	15.26	14.13 (5.61) <sup>†</sup>	8.28 (5.02)	$2.26 \times 10^{11}$	$1.78 \times 10^5$
1(b)	4.80	16.92	6.46 (2.33)	2.31 (1.83)	1,216.68	62.45
1(c)	2.09	6.91	11.10 (4.75)	5.35 (3.21)	16,443.81	404.23
1(d)	2.05	9.85	11.04 (3.01)	5.78 (2.4)	4,829.58	147.86
2(a) <sup>‡</sup>	11.58	13.68	4.31 (2.11)	2.31 (1.41)	17.30	0.91
2(b) <sup>‡</sup>	5.86	13.53	5.79 (1.89)	2.97 (1.44)	58.67	2.22
2(c)	4.48	2.07	7.11 (2.80)	6.07 (1.38)	176.44	41.86
2(d) <sup>‡</sup>	12.06	15.04	4.56 (2.18)	2.76 (1.67)	22.16	1.85
3(a) <sup>‡</sup>	2.20	N/A	39.8* (0.79)	37.7* (0.27)	0.58	0.0
3(b) <sup>‡</sup>	2.47	N/A	41.6* (0.87)	N/A	14.69	N/A

Expt = experiment; N/A = not available.

Physiologic CEM43 was calculated by offsetting the mean temperature elevation by  $37^\circ\text{C}$  in experiments 1 and 2 to reflect a physiologic baseline temperature. Temperatures for preclinical experiments (experiments 1 and 2) are expressed as temperature increases from baseline ( $\Delta T^\circ\text{C}$ ). Temperatures for clinical treatments (experiment 3) are expressed as absolute temperatures.

\* Absolute temperature.

<sup>†</sup> Standard deviations in parentheses.

<sup>‡</sup> Ribs present.

the potential ability to treat larger tumours to completion clinically because of the shorter half-life of circulating drug. Coverage time was reduced to just 35 min using a wider dot interval of 4 mm with the same row separation, requiring 13.8/7.6 kJ (432 s of HIFU time  $\times$  32 W in continuous wave) for a  $\Delta T$  of  $5^\circ\text{C}$ – $10^\circ\text{C}$  in the absence of ribs (experiment 1b, Fig. 4b). In both cases of 2- and 4-mm dot separation, the minimum on:off time of 1 s each was used for each unit, and unit–unit transducer translation time was around 2 s on average. This resulted in repetitions of 1 s on, 1 s off, 2 s move and pause, which means over the entire volume, the prescribed continuous wave (100% DC) during “on” time was thus reduced to an effective DC of approximately 20%.

By contrast, linear mode at a prescribed DC of 25% covered the same target volume in less than 15 min and slightly exceeded the maximum desired  $\Delta T$  while requiring only 4.2/2.3 kJ, representing a dramatic improvement in time and energy efficiency for volumetric hyperthermia (experiment 1c, Fig. 4c). By use of this optimised linear mode, refined control of  $\Delta T$  over a prolonged period  $>45$  min could be achieved by lowering the DC from 25% for the initial induction phase of 15 min to lower values for maintenance. The modest increase in temperature during the maintenance phase reflects that the device is running at the lowest possible output power (32 W) and stable DCs (6%–10%), because of a lack of attenuating overlying tissues and ribs. In this case, the FOH recorded a comparable  $\Delta T$  profile, validating the TM readings by an independent method (experiment 1d, Fig. 4d). The closely matched heating profiles between the fine FOH and the metallic and more bulky adjacent thermistors also suggests that thermocouple artefact (Hynynen et al. 1983; Morris et al. 2008) is not a

significant contributing factor in monitoring bulk heating using this linear mode strategy.

In summary, at fixed power, linear mode volume coverage over a single treatment cycle was achieved in just under half the time relative to dot mode with a 4-mm interval, for more marked hyperthermia gains at only a fraction of the prescribed DC (25% vs. 100%). Thus, linear mode is a much more efficient mode of heat deposition.

#### Experiment Set 2: Effect of thermistor angle, ribs and treatment volume

Figure 5 provides the temperature histories for prescribed volumes of  $39\text{ cm}^3$  versus  $92\text{ cm}^3$  with and without ribs and at varied thermistor trajectories, along with the target elevation ( $\Delta T$ ) range shown in green and exposure metrics in the upper left. In the  $39\text{-cm}^3$  volume, for the same input energy (8.4/4.6 kJ) in linear mode, the presence of ribs reduced the resultant  $\Delta T$  by more than 50% (experiment 2a, Fig. 5a, relative to experiment 1c, Fig. 4c, where some overheating was observed). With refined DC control, the optimal range of hyperthermia ( $\Delta T = 4^\circ\text{C}$ – $8^\circ\text{C}$ ) was achieved centrally in  $<8$  min and peripherally in  $<30$  min and easily sustained (experiment 2b, Fig. 5b). Without ribs, a larger prescribed volume of  $92\text{ cm}^3$  was covered in 32 min and the angle of the TM was found to be inconsequential, further validating its use in clinical cases (experiment 2c, Fig. 5c). In the presence of ribs, it was possible to achieve satisfactory hyperthermia across the extent of this larger volume in less than 30 min (experiment 2d, Fig. 5d). In broad terms, the presence of ribs increased the time to achieve the hyperthermia threshold in the periphery from approximately 5 to 15 min and reduced the mean temperature

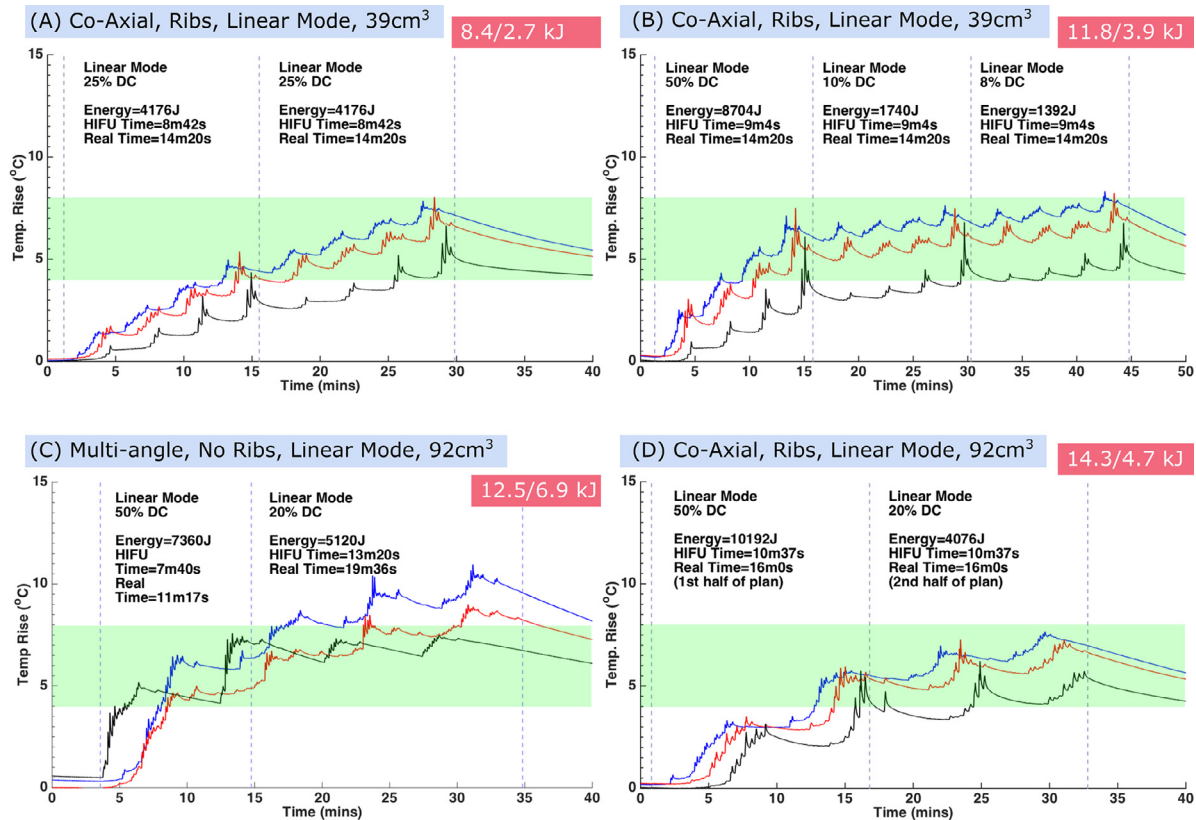


Fig. 5. Thermometry traces obtained from several *ex vivo* liver preparations in the presence of ribs, with the exception of (C), shown as a temperature increase ( $\Delta T$ ) from room temperature. Plots obtained in co-axial thermistor configuration (Fig. 1) with the exception of (C) which was performed in the multi-angled (0, 45°, 90°) configuration (Fig. 3). Green shaded regions represent target range of hyperthermia ( $\Delta T = 4^\circ\text{C} - 8^\circ\text{C}$ ). The blue trace represents centrally located and co-axially loaded reference thermistor; the red and black traces represent peripheral thermistors. Horizontal blue dashed lines represent start and end of focused ultrasound (FUS) cycles (a, b) or modification of duty cycle (DC) (c, d). Energy inputs are displayed as *a/b* kJ, where *a* = input energy obtained from JC200 treatment reports generated on JC200 device (HIFU seconds \* watts) and subsequently corrected for DC, and *b* = energy derated for soft tissues and ribs where present. High-intensity focused ultrasound (HIFU) time refers to the time when the transducer is delivering energy as if continuous wave and disregards DC. (a–d) Multiple treatments in linear mode, indicating the utility of DC modifications to induce and sustain central and peripheral hyperthermia. In particular, plot (b) indicates rapid induction (<15 min) and subsequent maintenance of a prolonged period of hyperthermia (for 30 min). Plot (c) indicates heating of a larger volume (92 cm<sup>3</sup>) in the absence of ribs, with some temperature overshooting in the maintenance phase; an output DC of 8%–10% would have been more controlled than the 20% DC used. The traces obtained with the different thermistor angulations (red, black) reveal no obvious variations from the co-axial trace (blue) to suggest effects in significant heating artifact. Plot (d) indicates how controlled hyperthermia can be induced and maintained in the larger volume, in the presence of ribs.

increase reached in the centre of the volume by approximately twofold for a fixed FUS exposure protocol.

#### Experiment set 3: Clinical effects including perfusion

In Figure 6 are real-time thermometry traces acquired for two different patients treated on the clinical trial. Dot mode was able to span the smaller (10.5 cm<sup>3</sup>) and superficial (centre at 46.5 cm depth) tumour volume in around 25 min, and at the slightly higher power of 50 W, a temperature consequent with release was achieved in around 4 min (experiment 3a, Fig. 6a). Of note the thermistor placed just peripherally to the tumour

indicates an approximate 1°C temperature rise during exposure, reflecting the localised thermal effects of HIFU. Linear mode was able to span the much larger (73.4 cm<sup>3</sup>) and deeper (centre at 86-mm depth) tumour volume in a similar time frame, achieving adequate temperatures also within 4 min (experiment 3b, Fig. 6b). Subsequent DC modifications for partial cycles were then used to avoid overheating. For both experiments, temperatures in excess of the drug release threshold of 39.5°C were achieved for approximately 23 and 63 min, respectively. The rapid cool down at the end of heating in the second experiment (Fig. 6b) was due to removal of the thermistor from the

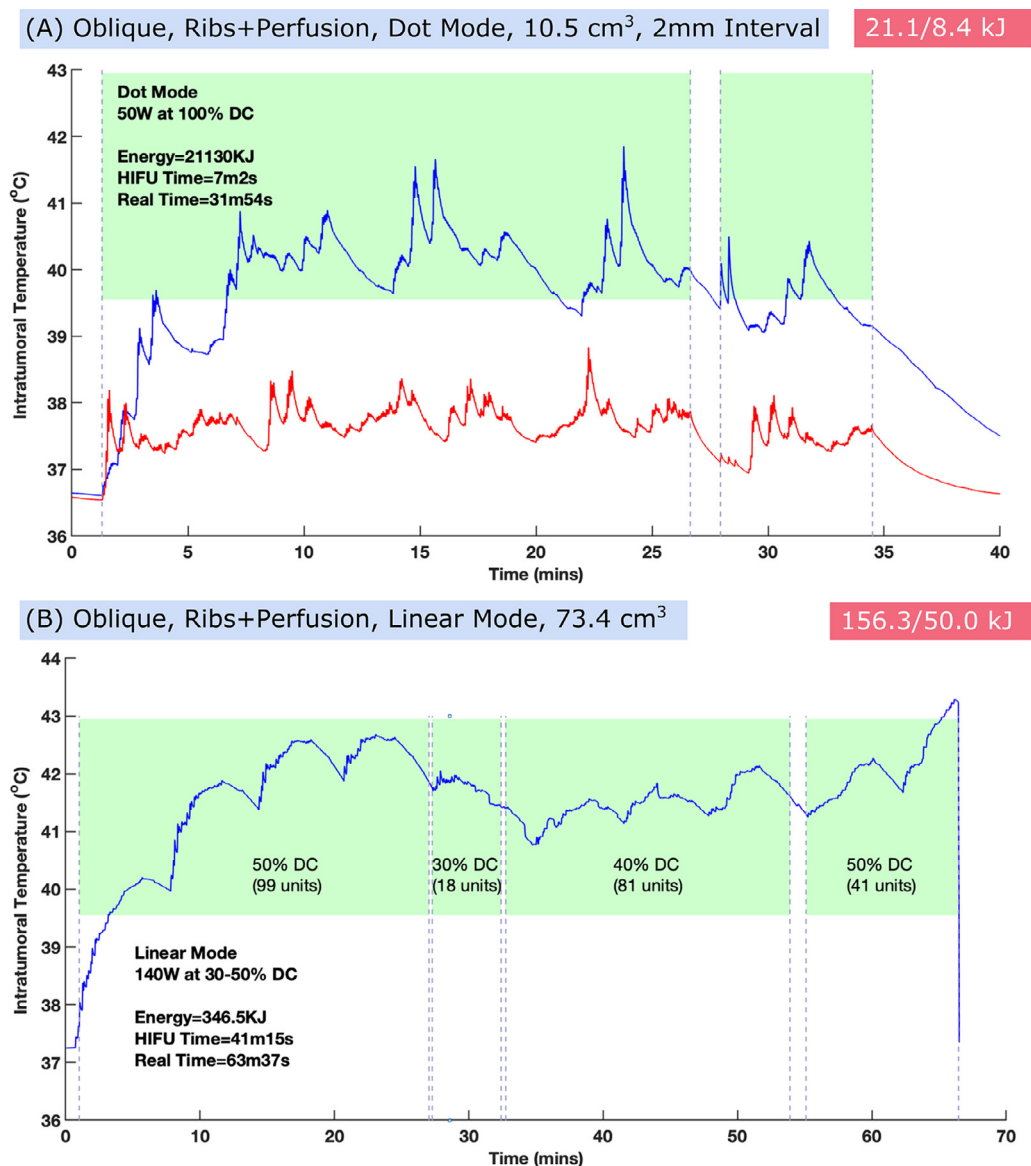


Fig. 6. Thermometry traces obtained intratumorally from clinical cases in the presence of ribs and perfusion, shown as absolute temperature. Plots obtained in oblique thermistor configuration. *Green shaded regions* represent the clinical target range of hyperthermia ( $T = 39.5^{\circ}\text{C} - 43^{\circ}\text{C}$ ). Energy inputs are displayed as  $a/b$  kJ, where  $a$  = input energy obtained from JC200 treatment reports generated on JC200 device (high-intensity focused ultrasound [HIFU] seconds \* watts) and subsequently corrected for duty cycle (DC), and  $b$  = energy derated for soft tissues and ribs where present. HIFU time refers to time when the transducer is delivering energy as if continuous wave, and disregards DC. (a) Thermometry acquired in dot mode for a smaller, superficial tumour. The *blue trace* represents the thermometry by the central intratumoral thermistor, and the *red trace*, a peripheral thermistor just outside the tumour margin. (b) Thermometry acquired in linear mode for a larger, deeper tumour. In both cases adequate hyperthermia was achieved quickly (within 4 min) and could be sustained for prolonged periods, consequent with drug release.

patient at the end of anaesthesia. For the second case, a larger derated energy of 50 kJ (compared with 8.4 kJ for the first clinical case) was required, given the sevenfold increase in tumour volume.

In Figures 7 and 8 are the fluorescence microscopy images of tumour biopsy samples obtained on the clinical trial for two different patients with metastatic

colorectal adenocarcinoma to the liver. The microscopy analysis reveals the spatial distribution of doxorubicin within the targeted liver metastases, with Figure 7 microscopy correlating to the same tumour whose thermometry trace is shown in Figure 6(A). In particular, the figures indicate the absence of intratumoral doxorubicin in the control biopsy before administration of



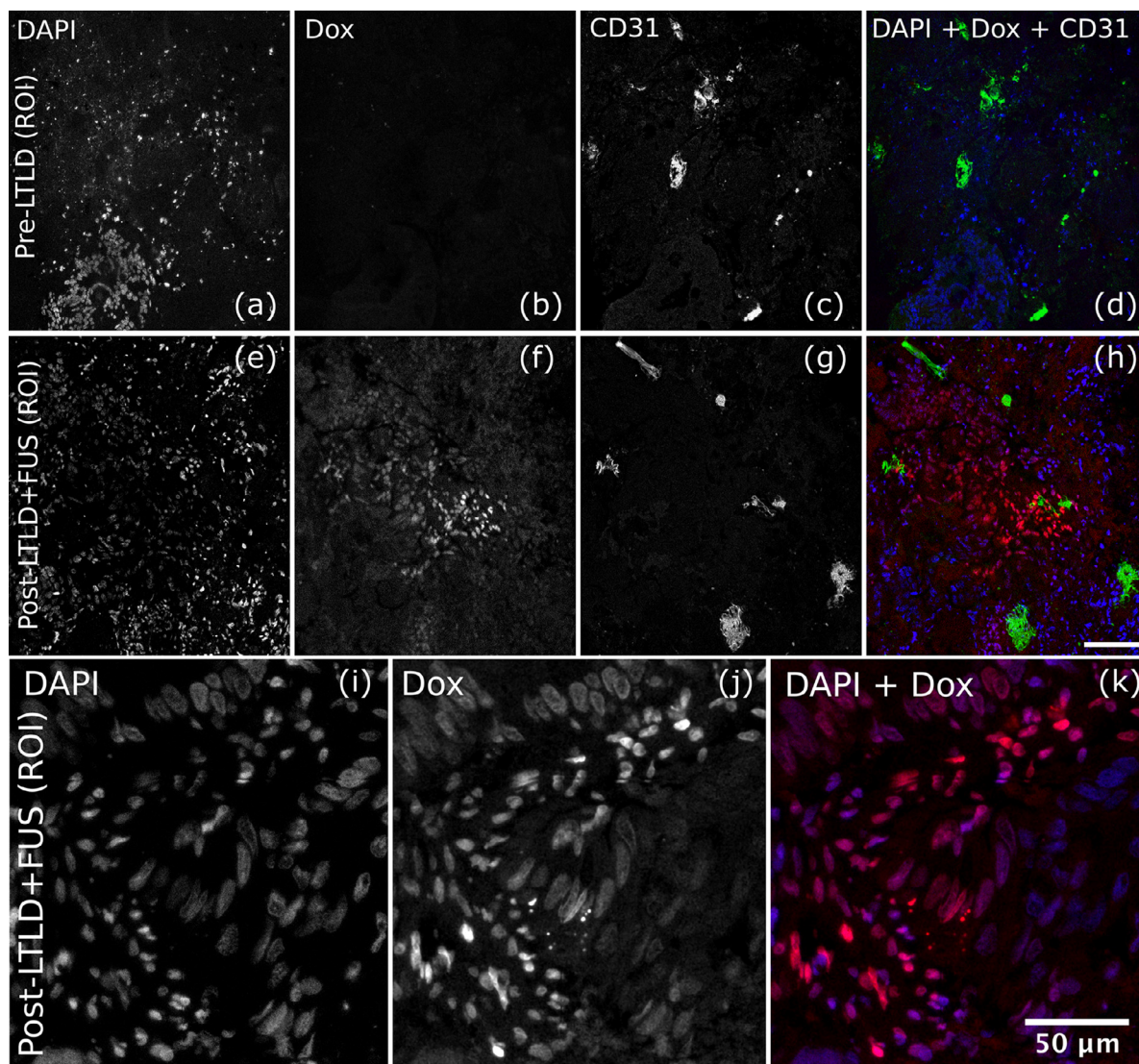


Fig. 7. Fluorescence microscopy study of vascular regions of interest (ROIs) of biopsies of colorectal adenocarcinoma metastatic liver tumours exposed to focused ultrasound (FUS) hyperthermia, obtained before drug (lyso-thermosensitive liposomal doxorubicin [LTLD]) (a–d) and after LTLD + FUS hyperthermia (e–k), for the same clinical case as per thermometry of Figure 6b. Samples were fixed in formalin and embedded in paraffin before reading. Images obtained by spectral un-mixing using published doxorubicin fluorescence signature, using Zeiss 710 confocal microscope with 100- $\mu\text{m}$  scale bar (a–h) and 50- $\mu\text{m}$  scale bar (i–k). The microscopy analysis reveals the presence of nuclear (bioavailable) doxorubicin in higher concentrations in the region of interest containing several vessels, with doxorubicin distributed to at least 300  $\mu\text{m}$  from closest vessel. Doxorubicin was present at much lower levels in necrotic and avascular tumour regions of the same sample using this technique. (a–d) The control biopsy before administration of LTLD reveals DAPI nuclear stain and CD31 vascular stain (*blue* and *green* in (d) respectively), with expected absence of doxorubicin fluorescence. (e–h) The biopsy obtained after LTLD + FUS hyperthermia revealed doxorubicin fluorescence of highest signal centrally within the vascular ROI, which appears to correlate (and indeed compete) with DAPI nuclear stain. (i–k) A closer look at a smaller region within the ROI of the same LTLD + FUS biopsy sample confirms co-localisation of nuclear DAPI stain (*blue* in [k]) with doxorubicin fluorescence (*red* in [k]), indicating that the doxorubicin is bioavailable (released from the lyso-thermosensitive liposome), subsequently diffusing into the cells and ultimately becoming nuclear bound. (Figure reproduced from Lyon *et al.*, 2018, Supplementary Material, with minor modification, with permission).

drug, minimal intratumoral doxorubicin after LTLD alone and widespread intratumoral doxorubicin after LTLD + FUS hyperthermia. Of crucial importance, doxorubicin was found to spatially correlate, and

indeed compete, with the DAPI (4',6-diamidino-2-phenylindole) nuclear counterstain, indicating that bioavailable doxorubicin had been released from the liposomes, allowing intracellular diffusion and



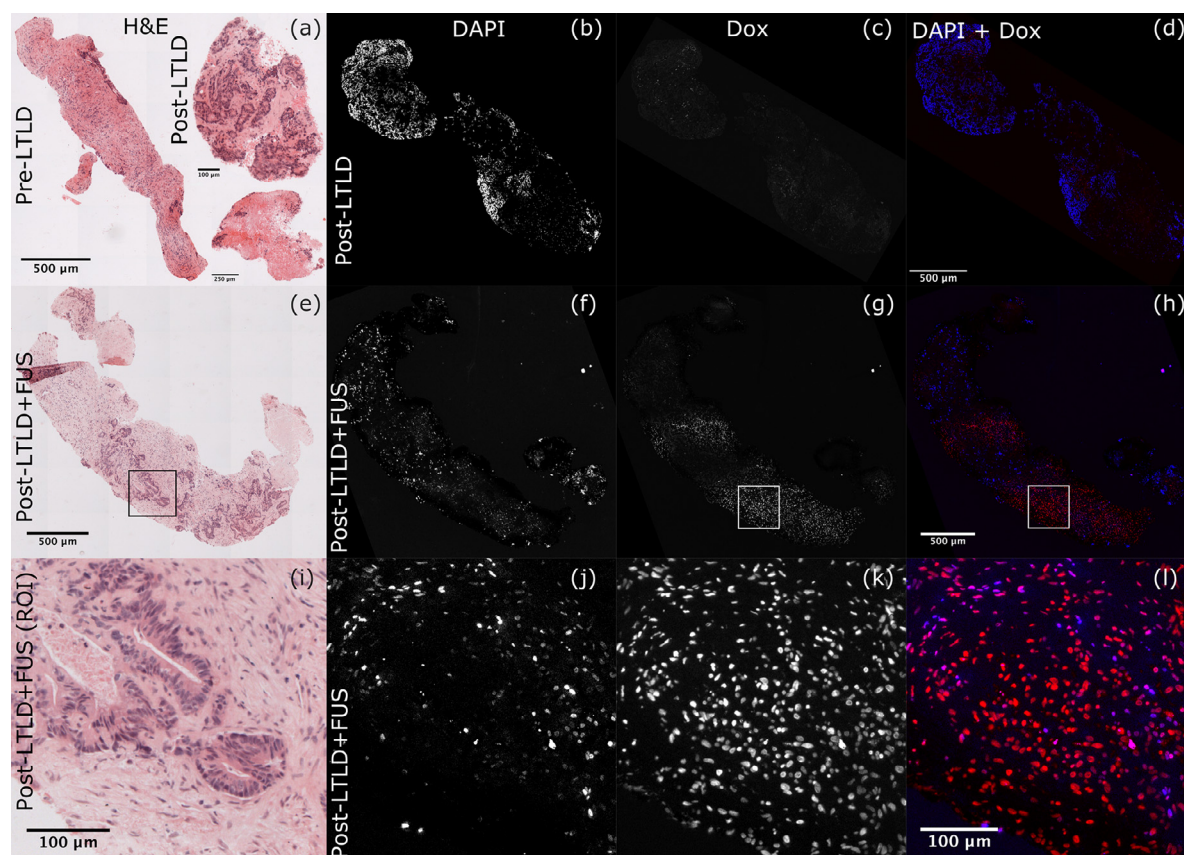


Fig. 8. Haematoxylin and eosin (H&E) staining and fluorescence microscopy study of biopsies of colorectal adenocarcinoma metastatic liver tumour exposed to focused ultrasound (FUS) hyperthermia, obtained before drug (lyso-thermosensitive liposomal doxorubicin [LTLD]) (a), after LTLD infusion (a–d) and after LTLD + FUS hyperthermia (e–l), for a different patient receiving the TARDOX study intervention. (a–d) Despite extensive nuclear staining with DAPI, a minimal doxorubicin signal is observed within the tumour sample obtained after LTLD but before FUS hyperthermia. (e–h) Widespread doxorubicin staining is observed throughout the tumour sample obtained after LTLD + FUS hyperthermia. (i–l) In a region of interest of the sample obtained after LTLD + FUS hyperthermia, co-localisation of DAPI and doxorubicin fluorescence is again observed, indicating bioavailable nuclear doxorubicin. (Figure reproduced from Lyon et al., 2018, Supplementary Material, with minor modification, with permission).

subsequent nuclear binding. Further, doxorubicin was noted to be in highest concentrations (fluorescence signal intensity) in the more vascular regions of the tumour relative to avascular regions. In these two cases, analytical lab quantification revealed an increase in the total concentration of intratumoral doxorubicin from 1.59 to 2.09  $\mu\text{g/g}$  and from 2.23 to 11.50  $\mu\text{g/g}$  before and after FUS hyperthermia, respectively. The minimal increase in intratumoral concentration in the former case is thought to be caused by biopsy of a highly necrotic region of tumour, where only minimal foci of vasculature staining (CD31) were seen. Overall, across the 10 patients treated, the clinical study found an average increase of 3.7 times in intratumoral biopsy doxorubicin concentrations, from an estimate of 2.34  $\mu\text{g/g}$  (standard deviation 0.93) immediately after LTLD infusion to 8.56  $\mu\text{g/g}$  (5.69) after FUS, meeting the primary endpoint of the trial (Lyon et al. 2018).

### Safety

After these controlled hyperthermia experiments, none of the exposure parameters in Table 2 resulted in either gray-scale changes on the JC200 B-mode images or, for the pre-clinical cases, visible ablative damage when the liver was sectioned and examined macroscopically. However, in interpretation of this result, one must be aware that the baseline temperature of the liver was at room temperature, well below physiologic temperatures; thus, ablative damage becomes much less likely for these small temperature increases.

Perhaps unsurprisingly, in the absence of ribs and other superficial attenuating tissues and at these shallow depths, the high intensities produced by the JC200 at minimal power (32 W) and DCs (6%–25%) produced unacceptably high temperature elevations beyond desired levels of mild hyperthermia (experiment 1a, 1c, 1d and experiment 2c). When temperature traces were

offset to a baseline (physiologic) 37°C, CEM43 values were well above the 240-min limit quoted for thermal ablation (Table 3) (Sapareto and Dewey 1984). However, in a more realistic thoracic treatment scenario including ribs in the propagation path, the proposed heating protocol produces hyperthermia (Fig 4) and cumulative exposure that are in desired and tolerable ranges (adjusted CEM43 range: 17.3–58.7 min; Table 3) and, with power increases, easily translatable to greater depths as typically required clinically.

For the clinical cases, no skin burns were observed and contrast-enhanced MRI the day after HIFU treatment revealed no evidence of thermal ablation (Lyon *et al.* 2018). Despite increased power, CEM43 was well within acceptable limits for the clinical cases (0.3 and 13.1 min), presumably attributable to perfusion and attenuation effects (Lyon *et al.* 2018).

### Limitations

Limitations of the *ex vivo* model are as follows:

1. The subphysiologic baseline temperature (room temperature) was required because of the practical limitations of experimental setup. However, if the baseline environmental temperature was fixed and conductive losses could be ignored, in perfect equilibrium the energy required to raise a volume from 22°C to 26°C is equivalent to that required to heat the same volume from 37°C to 41°C, as the specific heat is unchanged.
2. The absence of perfusion effects (both macro- and microvasculature) and the insulating effect of the Delrin custom holder both serve to reduce the rate of heat loss from the tissue sample, meaning that temperature increases obtained in the preclinical experiments are likely to overestimate those seen in clinical cases at the same parameters (power, DC), ignoring superficial attenuating tissues.
3. Absence of translational effects of the liver which would be encountered by respiratory motion. In the clinical study, liver motion was minimised to millimetric levels using the technique of high-frequency jet ventilation whilst the patient was under a general anaesthetic (Lyon *et al.* 2018).
4. There is a lack of significant depth of liver tissue penetration to the target and inclusion of only ribs and normal liver parenchyma in the preclinical model. The deeper tissue penetrance required in clinical cases with the presence of attenuating connective tissue layers, such as skin, fat, cartilage and potentially several more centimetres of normal liver, means that that significant compensatory power increases would be expected to achieve hyperthermia at depth in most clinical scenarios, as validated by the clinical results. Of note, the JC200 power output can be increased to up to 350 W, a

greater than tenfold increase over the minimum power level of 32 W used in this *ex vivo* model.

5. In the absence of volumetric MR thermometry, real-time thermometry monitoring was achieved in this study using invasive thermistors in the centre and periphery of the heated field. Whilst high-resolution regional temperature mapping is not possible, the method has the advantage of affording practicality in terms of translation to clinical treatments without the requirement for MRI.

These limitations highlight the importance of clinical validation of real-time intratumoral thermometry in early FUS drug delivery studies employing thermosensitive agents. This may be achieved through non-invasive MR thermography (Staruch *et al.* 2011, 2015) or minimally invasive methods such as intratumoral thermistor implantation, as described here. The clinical data presented address limitations 1–4, and the final limitation is of questionable importance particularly in smaller tumour volumes (*e.g.*, <30 cm<sup>3</sup>), given that the intratumoral temperature attained from a central thermistor is likely to reflect an average or bulk temperature encompassing small microregional variations and that the optimum temperature range for LTLT release is broad (39.5°C–43°C). For larger tumour volumes (*e.g.*, 30–100 cm<sup>3</sup>), the hyperthermia profiles may be more complex as heating becomes less uniform, for example, between deep and superficial parts of the volume at the same output parameters.

### CONCLUSIONS

By optimising heating strategies of an ultrasound-guided clinical FUS device (JC200), we have determined the feasibility of rapidly induced, controlled and sustained large-volume tissue hyperthermia both in an *ex vivo* liver model in the presence of acoustically blocking ribs and subsequently in a clinical setting. Further, by establishing a useful set of system parameter settings such as speed, scan geometry and slice thickness, the number of degrees of freedom to be optimised for patient-specific treatment plans is reduced.

Preclinical optimisation was ultimately achieved using automated linear mode (moving beam) treatment plans at a low fixed power, with dynamic DC modification according to real-time thermometry. Without ribs, continuous wave dot mode was found to raise the temperature of a 39-cm<sup>3</sup> volume to the target range both centrally and peripherally after around 25 min (Fig. 4b) equating to 9.9 kJ (13.8 kJ of input energy over 35 min, thus an estimated 13.8 \* 25/35 kJ over the first 25 min). This is equivalent to 7.6 \* 25/35 = 5.4 kJ derated energy in 25 min. Low-DC linear mode achieved the same outcome at the same power setting (“32 W”) after approximately 10 min (Fig. 4c) using just 2.8 kJ (8.4 kJ \* 10/30

min)/1.5 kJ. In the largest attempted target volume of 92 cm<sup>3</sup>, controlled hyperthermia was induced within 15 min using 10.2/3.3 kJ and sustained over a further 15 min using 4.1/1.3 kJ in linear mode in the presence of ribs, a total of 4.6 kJ of derated energy (Fig. 5d). This compares with the 13.8/7.6 kJ of energy required to induce and sustain similar levels of hyperthermia in dot mode over the same period over a smaller 39-cm<sup>3</sup> volume even in the absence of ribs. The significantly improved heating efficiency in linear mode is understood to be largely due to minimising the “off” dwell time, an opportunity for cooling in dot mode hyperthermia.

The limitations of this *ex vivo* model collectively serve to underrepresent both the attenuation and conductive cooling effects, which are much more significant clinically, accounting for the higher derated energy requirements clinically. The clinical data indicate that, despite perfusion effects, for larger tumour volumes up to 74 cm<sup>3</sup> in depth, adequate central hyperthermia can be achieved in <4 min using linear mode, with full tumour coverage in 25 min.

## DISCUSSION

A major clinical challenge of non-invasive FUS-induced hyperthermia for drug delivery is the difficulty in maintaining homogeneous local temperature up to 43°C for 30–60 min within a targeted cancer. Several *in vivo* studies have found that at temperatures >43°C, tumour perfusion may begin to decrease (Brown et al. 1992; Song et al. 2005), thus hindering the delivery of a systemic agent and emphasising the need for controlled levels of hyperthermia.

MR-guided heating strategies for hyperthermia have been under investigation for more than two decades and have the advantage of providing beam-steering and non-invasive real-time thermography using multi-element arrays (Diederich and Hynynen 1999; Köhler et al. 2009; Staruch et al. 2011; Grull and Langereis 2012; Tillander et al. 2016). One study reported large-volume hyperthermia in an *in vivo* porcine leg model using an MR-guided FUS device and achieved volumetric hyperthermia of comparable magnitudes for durations up to 60 min using both electronic and mechanical beam translation, without acoustically blocking ribs (Tillander et al. 2016).

Such MR-guided devices, however, come at considerable cost and have practical limitations because of the constraints of the MRI tunnel, whereas future ultrasound-guided FUS devices designed for hyperthermia may become portable. Further, the running costs of ultrasound-guided FUS devices are considerably lower than the overheads of MR-guided systems, making them an economically more attractive alternative for high throughput of targeted treatments. In addition,

ultrasound-guided devices may offer practical benefits, for example, facilitating interventions such as peri-procedural biopsy (Lyon et al. 2017).

The focal volumes of conventional clinical HIFU ablative devices, such as that used in the present study, are orders of magnitude smaller than clinical tumour volumes. Further, because of the heterogeneity of tumour vasculature, microregional variations in temperature rises across the target volume are inevitable. However, given the relatively generous target range for release of LTSs (typically between 39.5°C and 43°C), this may not pose a major clinical problem for large tumour volumes.

To the author's knowledge, building on an *ex vivo* tissue model with ribs, a strategy for attaining sustained large-volume hyperthermia (on the order of 10–100 cm<sup>3</sup>, applicable to tumour diameters up to 5–6 cm<sup>3</sup>) using the capabilities of an existing ultrasound-guided clinical HIFU system (JC200) has been implemented clinically for the first time. More specifically, despite the limitations of the single-element motorised transducer and small focus (transverse 3-dB beamwidth of 1.2 mm and an axial 3-dB length of 9.5 mm), the use of linear mode at a fixed FUS power and variable DC has been found to generate controlled volumetric hyperthermia in a more energy- and time-efficient manner than dot mode.

The strategy presented has been successfully translated clinically five of six patients in the first part of the TARDOX study, which used implanted thermistors (Lyon et al. 2018), and intratumoral hyperthermia traces for two of the patients are presented here along with selected microscopy imaging revealing the intratumoral distribution of doxorubicin. After these clinical treatments, the real-time thermometry acquired has been used to generate predictive models for varied tumour anatomies using computed tomography data, to treat patients completely non-invasively without thermometry in the second part of the study (Lyon et al. 2018; Gray et al. 2019). In this clinical study, liver tumours were heated in the presence of circulating LTLD, and tumour biopsies were used to quantify intratumoral drug delivery, causing an increase by an average of 3.7-fold pre- and post-FUS in addition to localised positron emission tomography–computed tomography response in several otherwise refractory target tumours. Thus, the non-invasive targeted intratumoral delivery of enhanced chemotherapy concentrations consequent with single-cycle chemo-ablation may now be in grasp without the requirement for MR thermometry.

After clinical validation of the heating strategy presented (Gray et al. 2019), it is anticipated that the same approach may be applied to other clinical studies involving hyperthermia-mediated chemotherapeutics across a range of tumour indications. The future may see development of portable and non-portable ultrasound-guided FUS



devices specifically designed for hyperthermia across a range of indications including targeted chemotherapy.

**Acknowledgments**—The authors acknowledge Jim Fisk and David Salisbury of the Institute of Biomedical Engineering, University of Oxford, for fabricating phantoms used in the experiments. We acknowledge Mutchmeats Ltd., Oxfordshire, a local abattoir and wholesale butcher, for providing bovine liver. Finally, we acknowledge Haifu Medical, Chongqing, China, for manufacturing and supporting the JC200 clinical device in Oxford.

The research was funded by the National Institute for Health Research (NIHR) Oxford Biomedical Research Centre (BRC) based at Oxford University Hospitals NHS Foundation Trust and University of Oxford. The views expressed are those of the author(s) and not necessarily those of the NHS, NIHR or Department of Health.

**Conflict of interest disclosure**—The authors report no conflicts of interest.

## REFERENCES

- Bennewith KL, Dedhar S. Targeting hypoxic tumour cells to overcome metastasis. *BMC Cancer* 2011;11:504.
- Brown SL, Hunt JW, Hill RP. Differential thermal sensitivity of tumour and normal tissue microvascular response during hyperthermia. *Int J Hyperthermia* 1992;8:501–514.
- Chao YT, Hsu CJ, Yu YL, Yen JY, Ho MC, Chen YY, Chang HC, Lian FL. A novel sound-blocking structure based on the muffler principle for rib-sparing transcostal high-intensity focused ultrasound treatment. *Int J Hyperthermia* 2015;31:507–527.
- Diederich CJ, Hynynen K. Ultrasound technology for hyperthermia. *Ultrasound Med Biol* 1999;25:871–887.
- Gray MD, Lyon PC, Mannaris C, Folkes LK, Stratford M, Campo L, Chung DYF, Scott S, Anderson M, Goldin R, Carlisle R, Wu F, Middleton MR, Gleeson FV, Coussios CC. Focused ultrasound hyperthermia for targeted drug release from thermosensitive liposomes: Results from a phase I trial. *Radiology* 2019;291:232–238.
- Grull H, Langereis S. Hyperthermia-triggered drug delivery from temperature-sensitive liposomes using MRI-guided high intensity focused ultrasound. *J Control Release* 2012;161:317–327.
- Hasgall P, Di Gennaro F, Baumgartner C, Neufeld E, Lloyd B, Gosselin M, Payne D, Klingensböck A, Kuster N. IT<sup>2</sup>IS database for thermal and electromagnetic parameters of biological tissues, Version 4.0 [online]. [www.itis.ethz.ch/database](http://www.itis.ethz.ch/database). Accessed January 8, 2021.
- Hill CR, ter Haar GR. Review article: High intensity focused ultrasound—Potential for cancer treatment. *Br J Radiol* 1995;68:1296–1303.
- Hynynen K, Martin CJ, Watmough JB, Mallard JR. Errors in temperature measurement by thermocouple probes during ultrasound induced hyperthermia. *Br J Radiol* 1983;56:969–970.
- Illing RO, Kennedy JE, Wu F, Ter Haar GR, Protheroe AS, Friend PJ, Gleeson FV, Cranston DW, Phillips RR, Middleton MR. The safety and feasibility of extracorporeal high-intensity focused ultrasound (HIFU) for the treatment of liver and kidney tumours in a Western population. *Br J Cancer* 2005;93:890–895.
- Jain RK. The next frontier of molecular medicine: Delivery of therapeutics. *Nat Med* 1998;4:655–657.
- Jain RK. Delivery of molecular and cellular medicine to solid tumors. *Adv Drug Deliv Rev* 2012;64(Suppl):353–365.
- Kennedy JE, Ter Haar GR, Cranston DJ. High intensity focused ultrasound: Surgery of the future?. *Br J Radiol* 2003;76:590–599.
- Khokhlova TD, Wang YN, Simon JC, Cunitz BW, Starr F, Paun M, Crum LA, Bailey MR, Khokhlova VA. Ultrasound-guided tissue fractionation by high intensity focused ultrasound in an in vivo porcine liver model. *Proc Natl Acad Sci USA* 2014;111:8161–8166.
- Köhler MO, Mougenot C, Quesson B, Enholm J, Le Bail B, Laurent C, Moonen CTW, Ehnholm GJ. Volumetric HIFU ablation under 3D guidance of rapid MRI thermometry. *Med Phys* 2009;36:3521–3535.
- Kong G, Dewhurst MW. Hyperthermia and liposomes. *Int J Hyperthermia* 1999;15:345–370.
- Liu X, Yin C, Gong X, Cao W. Theoretical and experimental study on temperature elevation behind ribs caused by weakly focused ultrasound. *Ultrasound Med Biol* 2010;36:1704–1712.
- Lyon PC. Targeted release from lyso-thermosensitive liposomal doxorubicin (ThermoDox) using focused ultrasound in patients with liver tumours. Thesis. : University of Oxford; 2016.
- Lyon PC, Griffiths LF, Lee J, Chung D, Carlisle R, Wu F, Middleton MR, Gleeson FV, Coussios CC. Clinical trial protocol for TARDOX: A phase I study to investigate the feasibility of targeted release of lyso-thermosensitive liposomal doxorubicin (ThermoDox) using focused ultrasound in patients with liver tumours. *J Ther Ultrasound* 2017;5:28.
- Lyon PC, Gray MD, Mannaris C, Folkes LK, Stratford M, Campo L, Chung DYF, Scott S, Anderson M, Goldin R, Carlisle R, Wu F, Middleton MR, Gleeson FV, Coussios CC. Safety and feasibility of ultrasound-triggered targeted drug delivery of doxorubicin from thermosensitive liposomes in liver tumours (TARDOX): A single-centre, open-label, phase 1 trial. *Lancet Oncol* 2018;19:1027–1039.
- Lyon PC, Rai V, Price N, Shah A, Wu F, Cranston D. Ultrasound-guided high intensity focused ultrasound ablation for symptomatic uterine fibroids: Preliminary clinical experience. *Ultraschall Med* 2020;41:550–556.
- McGough RJ, Kessler ML, Ebbini ES, Cain CA. Treatment planning for hyperthermia with ultrasound phased arrays. *IEEE Trans Ultrason Ferroelectr Freq Control* 1996;43:1074–1084.
- Morris H, Rivens I, Shaw A, Ter Haar G. Investigation of the viscous heating artefact arising from the use of thermocouples in a focused ultrasound field. *Phys Med Biol* 2008;53:4759–4776.
- Needham D, Anyarambhatla G, Kong G, Dewhurst MW. A new temperature-sensitive liposome for use with mild hyperthermia: Characterization and testing in a human tumor xenograft model. *Cancer Res* 2000;60:1197–1201.
- Poon RT, Borys N. Lyso-thermosensitive liposomal doxorubicin: A novel approach to enhance efficacy of thermal ablation of liver cancer. *Expert Opin Pharmacother* 2009;10:333–343.
- Poon RT, Borys N. Lyso-thermosensitive liposomal doxorubicin: An adjuvant to increase the cure rate of radiofrequency ablation in liver cancer. *Future Oncol* 2011;7:937–945.
- Ren XL, Zhou XD, Zhang J, He GB, Han ZH, Zheng MJ, Li L, Yu M, Wang L. Extracorporeal ablation of uterine fibroids with high-intensity focused ultrasound: Imaging and histopathologic evaluation. *J Ultrasound Med* 2007;26:201–212.
- Sapareto SA, Dewey WC. Thermal dose determination in cancer therapy. *Int J Radiat Oncol Biol Phys* 1984;10:787–800.
- Smith SW, Pavy HG, von Ramm OT. High-speed ultrasound volumetric imaging system—Part I. Transducer design and beam steering. *IEEE Trans Ultrason Ferroelectr Freq Control* 1991;38:100–108.
- Song CW, Park HJ, Lee CK, Griffin R. Implications of increased tumor blood flow and oxygenation caused by mild temperature hyperthermia in tumor treatment. *Int J Hyperthermia* 2005;21:761–767.
- Staruch R, Chopra R, Hynynen K. Localised drug release using MRI-controlled focused ultrasound hyperthermia. *Int J Hyperthermia* 2011;27:156–171.
- Staruch RM, Ganguly M, Tannock IF, Hynynen K, Chopra R. Enhanced drug delivery in rabbit VX2 tumours using thermosensitive liposomes and MRI-controlled focused ultrasound hyperthermia. *Int J Hyperthermia* 2012;28:776–787.
- Staruch RM, Hynynen K, Chopra R. Hyperthermia-mediated doxorubicin release from thermosensitive liposomes using MR-HIFU: Therapeutic effect in rabbit Vx2 tumours. *Int J Hyperthermia* 2015;31:118–133.
- Tillander M, Hokland S, Koskela J, Dam H, Andersen NP, Pedersen M, Tanderup K, Ylihautala M, Köhler M. High intensity focused ultrasound induced in vivo large volume hyperthermia under 3D MRI temperature control. *Med Phys* 2016;43:1539.
- Wang K, Chen L, Meng Z, Lin J, Zhou Z, Wang P, Chen Z. High intensity focused ultrasound treatment for patients with advanced pancreatic cancer: A preliminary dosimetric analysis. *Int J Hyperthermia* 2012;28:645–652.
- Wood BJ, Poon RT, Locklin JK, Dreher MR, Ng KK, Eugeni M, Seidel G, Dromi S, Neeman Z, Kolf M, Black CDV, Prabhakar R, Libutti SK. Phase I study of heat-deployed liposomal doxorubicin during radiofrequency ablation for hepatic malignancies. *J Vasc Interv Radiol* 2012;23:248–255.e7.